FEDSM2003-45577

SIMULATIONS OF COMPLEX FLOWS AND FLUID-STRUCTURE INTERACTION PROBLEMS ON FIXED CARTESIAN GRIDS

Fady M. Najjar
Center for Simulations of Advanced Rockets
University of Illinois at Urbana-Champaign
1101 West Springfield Avenue, MC-278
Urbana, IL 61801, U.S.A.
e-mail: fnajjar@csar.uiuc.edu

Rajat Mittal
Department of Mechanical and Aerospace
Engineering
The George Washington University
Suite T729, 801 22nd St. NW
Washington, DC 20052, U.S.A.
e-mail: mittal@seas.gwu.edu

ABSTRACT

A finite-difference based approach for computing flows with complex moving solid three-dimensional boundaries on fixed Cartesian grid has been developed. Internal solid boundaries are represented by "blocking off" the grid cells inside the boundary. This results in considerably increased computing efficiency over conventional body-conformal structured grid methods. A mixed explicit-implicit fractional step method is employed for time integration while the spatial discretization scheme is based on a second-order accurate central-difference scheme. The pressure Poisson equation is solved using algebraic multigrid as well as Krylov subspace based methods. The current simulation methodology is validated by simulating various canonical flows. Further, we compute the flow generated by a moving body as well as the flow generated by a synthetic jet in order to demonstrate the capabilities of this solver.

INTRODUCTION

Direct numerical simulation (DNS) of flows with engineering relevance remains a challenging task with current computer hardware and software capabilities. Hence, some type of modeling or approximation is usually introduced into the flow computations in order to simplify them and make them feasible on existing computer platforms. Usually, the approximation is introduced in the representation of the turbulence scales in the form of a turbulence model which significantly reduces the spatial and temporal resolution requirements. In the conventional Reynolds Averaged Navier-Stokes (RANS) modeling approach which is heavily used in the engineering community, the model takes on the onus of representing the effect of all the turbulence fluctuations. Such modeling approach with its variants has been used extensively in a variety of flow configurations and seems to perform

adequately for many high Reynolds number attached flows. However, for separated flows, the predictive capability of this approach is significantly more limited. Furthermore, for problems involving fluid-structure interaction, the fidelity of this modeling approach remains to be fully demonstrated. An alternative to DNS is large-eddy simulation (LES) approach, which resolves the energy-containing turbulence scales while modeling the subgrid scales (SGS). LES provides provides information about a wide range of spatial and temporal scales in the flow at a cost that is significantly lower than DNS. However, LES computations of high Reynolds number flows with complex geometries still remain out of reach of present day computers.

For such flows, it seems worthwhile to explore other venues of simplifying the DNS/LES approaches as to retain their ability to resolve the temporal and spatial flow dynamics while reducing the computational resources required for these types of simulations. One approach is to simplify the specification of the solid boundary. To this end, a finite-difference based method has been developed to investigate flows with complex stationary and moving solid boundaries on fixed Cartesian grids. The key simplification is that any solid body configuration is represented through "blocking off" (also referred to as "iblanking") the Cartesian grid cells which lie inside the body; hence, the body surface is represented only in a C^0 continuous manner. Thus, in this method we sacrifice the ability to represent the body surface in a smooth manner. What we gain instead is a purely Cartesian nature to the governing equations offering tremendous advantages in terms of solver simplicity, parallelizability and efficiency. Fig. 1 shows the iblanking implemented for a circular cylinder embedded inside a Cartesian grid. It is noted that the boundary shape can be captured quite well on dense grids. Note that this simple

representation of the internal boundaries obviates the need for working with curvilinear structured or unstructured grids. Furthermore, complexities usually associated with conventional Cartesian grid methods [1] such as complex interpolation scheme, cut-cells and distributed body forces are also avoided. Clearly, this simplicity comes at the price of not being able to represent the body shape in a smooth manner. Due to this, one has to be careful in applying this approach to flows where the attached boundary layer on the internal boundary is turbulent. The objective of the current paper is to provide a preliminary assessment of such simulation a approach. In order to accomplish this, we have simulated a number of canonical flows and compared the results with well established experiments. Further, we present results for flows with moving boundaries as well as a relatively complex synthetic jet configuration.

MATHEMATICAL FORMULATION

The current numerical procedure solves the time-dependent conservative form of the three-dimensional mass and momentum equations for an incompressible fluid. The Navier-Stokes equations written in tensor form are:

$$\frac{\partial u_i}{\partial x_i} = 0$$

$$\frac{\partial u_i}{\partial t} + \frac{\partial u_i u_j}{\partial x_j} = -\frac{\partial p}{\partial x_i} + \frac{1}{Re}\frac{\partial^2 u_i}{\partial x_j \partial x_j} \qquad (1)$$

where the indices, $i=1,2,3$, represent the x (streamwise), y (cross-stream) and z (spanwise) directions, respectively; while the streamwise, cross-stream and spanwise velocity components are denoted by u (u_1), v (u_2) and w (u_3), respectively. The equations are nondimensionalized by the appropriate length and velocity scales with Re corresponding to the Reynolds number. The equations are integrated in time using the fractional step method [2]. This approach follows along the lines of that used by [3,4]. In the first step, an intermediate velocity field, $\widetilde{u}_i$, is calculated from the momentum equations without the contribution of the pressure gradient. In the second step, the pressure field is computed by solving a Poisson equation. The divergence-free velocity field, u_i^{n+1}, is then obtained by correcting the intermediate velocity field with the computed pressure gradient. In the current solution procedure, the convective terms are represented using an explicit Adams-Bashforth scheme; while the diffusive terms are modeled with an implicit Crank-Nicolson procedure. The temporally discretized momentum equations are written as:

$$\frac{\widetilde{u}_i - u_i^n}{\Delta t} = \frac{1}{2}\left(3N_i^n - N_i^{n-1}\right) + \frac{1}{2Re}\left(\widetilde{L}_i + L_i^n\right) \qquad (2)$$

where

$$N_i = \frac{\partial u_i u_j}{\partial x_j}$$

$$L_i = \frac{\partial^2 u_i}{\partial x_j \partial x_j} \qquad (3)$$

The divergence-free velocity field, u_i^{n+1}, satisfies

$$\frac{u_i^{n+1} - \widetilde{u}_i}{\Delta t} = -\frac{\partial p^{n+1}}{\partial x_i} \qquad (4)$$

and applying the divergence operator and invoking the continuity equation, the Poisson equation for the pressure field is derived to be:

$$\nabla \cdot \left(\nabla p^{n+1}\right) = \frac{1}{\Delta t}\left(\nabla \cdot \widetilde{u}\right) \qquad (5)$$

The spatial derivatives have been discretized with a second-order accurate central difference scheme on a collocated finite-difference stencil. In the collocated-grid arrangement, all variables (i.e., velocity components and pressure) are located at the same physical location in contrast to the staggered node arrangement where the velocities are centered with the pressure locations. For the pressure-Poisson equation (5), the gradient term uses a compact second-order central difference stencil. In addition to the cell-centered nodal velocities, we separately carry and update the face normal velocities. This permits to satisfy the divergence-free condition to machine accuracy (see Zang *et al.*, [5] for further details). An iterative line-Jacobi solver is invoked to solve Eq. (2); while the Pressure Poisson Equation (PPE) is solved using an Algebraic MultiGrid (AMG) solver. Recently, a generic flexible suite of solvers based on the PETSC library [6] has also been incorporated [7]. Furthermore, a variety of boundary conditions including uniform and time-dependent inflow, symmetry, and outflow, can be invoked during the solution procedure.

To permit the embedding of obstacles inside the computational domain, an "iblank" variable is defined for all the cells. This flag is set to a value of 1 for cells that are inside the boundary and equal to 0 for cells in the fluid. A fluid cell (with iblank=0) which has at least one neighbor inside the body (with iblank=1) is designated a "boundary cell" and the discretization of the equations is modified in these cells to account for the no-slip, no-penetration condition on the body. As with other Cartesian grid methods [1,8,9], the advantage of this approach is that very complex shaped bodies can be embedded in the grid without having to generate and work with complex grids. Furthermore, since the grid does not conform to the boundary shape, boundary motion can also easily be included.
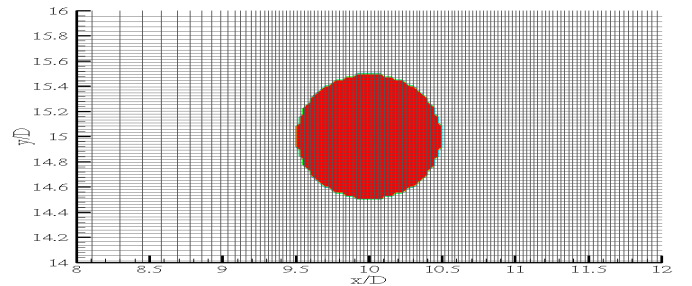
Fig. 1. Representation of the geometrical configuration through "blocking-off" grid cells for a single circular cylinder with grid overlay.

RESULTS
Backward Facing Step

The canonical flow initially investigated is the flow past a backward facing step. This geometrical configuration represents a good validation test case since the "iblanking" capability captures exactly the Cartesian nature of the step. The grid chosen consists of 198x39 nodes with non-uniformly distributed cells. The computational domain extends in the streamwise (x) direction up to 30 and in the cross-stream (y) direction to 2. The step height (S) is 0.9423. Blocking-off of the backward step extends from the inlet till x=8. Uniform streamwise velocity inlet is prescribed at x=0, no-slip conditions are imposed on y=0 and 2; while a convective boundary condition is applied at the outflow (x=30) boundary. Computations are performed for a variety of Reynolds numbers (based on the mean inlet velocity and inlet height). Fig. 2(a) presents the variation of the reattachment lengths with Reynolds numbers obtained from the current simulations. It is observed that the reattachment length increases monotonically with increasing Reynolds number. Also shown are the experimental results obtained by Armaly *et al.* [10]. The computations corroborate well with the experiments up to Re=389. Significant differences are seen for higher Reynolds numbers as the flow transitions to a three-dimensional state. Fig. 2(b) shows the instantaneous spanwise vorticity contours in the configuration considered. The recirculation bubble with instantaneous vortical structure is captured downstream of the step; while significant vorticity is seen emanating on the top wall.

(a)

(b)
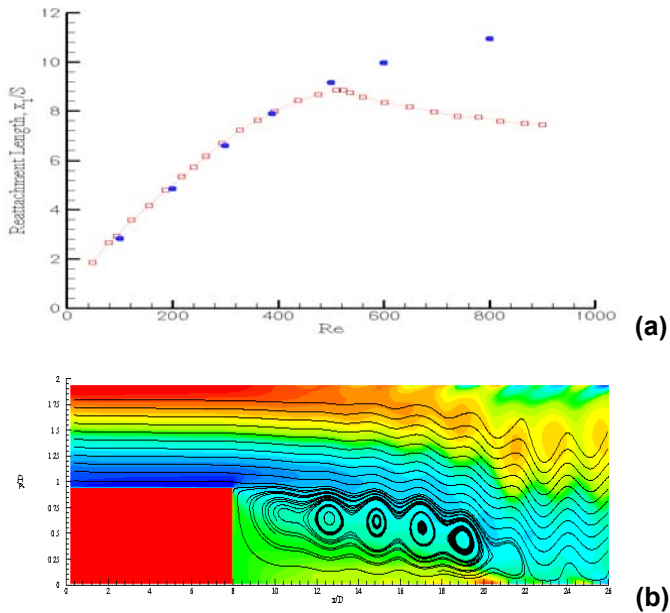
Fig. 2. (a) Distribution of the reattachment length with Reynolds number for flow past a backward facing step. Square symbols represent experimental data [10] and circle symbols correspond to current numerical results [7]; (b) Contours of instantaneous spanwise vorticity for flow past a backward facing step with streamline contours capturing the recirculation bubble.

Stationary Circular Cylinder

The second configuration chosen to validate the current computational capability is the flow past a stationary circular cylinder at low Reynolds number (Re=$U_\infty D/\nu$ where U_∞ is the free-stream velocity and D the cylinder diameter) of Re=100 and 200. The computations are carried out on a $30D \times 30D$ computational domain and the cylinder center, is located at (10D,15D). At the inflow (x=0), the bottom (y=0) and top (y/D=30) boundaries, a uniform free-stream velocity is imposed; while a convective boundary condition is applied at the outflow (x/D=30) boundary. The computational grid consists of 240x120 cells and the time step size, Δt, is set to 5×10^{-3}. The computations have been integrated temporally for over 20 shedding cycles and results analyzed subsequent to when the flow reaches a stationary state.

Fig. 3 presents contours of the instantaneous spanwise vorticity, ω_z, field for the flow past a circular cylinder at Re=200. The classical Karman shedding mechanism is well captured. Fig. 4 illustrates the temporal variations of the instantaneous lift, C_L, and drag, C_D, coefficients. The drag coefficient exhibits a dominant periodic time variation driven by the Karman vortex shedding process existing in the wake. Further, the lift coefficient is observed to have a zero time-mean value. The flow has been integrated over 350 nondimensional time units and statistics are gathered for the last 200 time units. The current computations predict a Strouhal number $\left(\text{St} = fD/U_\infty \right)$ of 0.20 corroborating with the value of 0.198 measured by Williamson [11]. The mean drag coefficient is computed to be 1.33, agreeing reasonably well with previous published values [8,12] of 1.35 and 1.38, respectively.
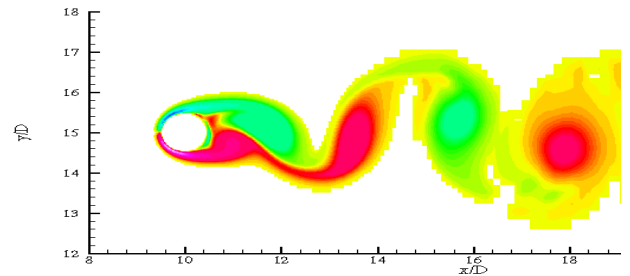
Fig. 3. Contours of instantaneous spanwise vorticity for flow past a circular cylinder at Re=200. Red (blue) values represent counterclockwise (clockwise) rotational motion.
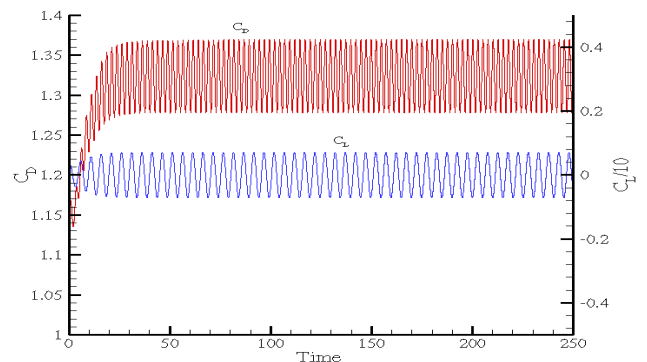
Fig. 4. Temporal evolution of lift and drag coefficients for flow past a circular cylinder at Re=200.

Fig. 5 presents contours of the root-mean-square (rms) of the streamwise velocity component. The profile is symmetric about the wake centerline with a maximum value of 0.47 close to the circular cylinder body. Also shown are the time-mean streamline contours. The mean wake bubble is clearly captured and has a length of 0.85D. Further, the base pressure coefficient (C_{pb}) is computed to be –0.693. This result compares well with the value of -0.6 computed by Braza *et al.* [12] for Re=100.
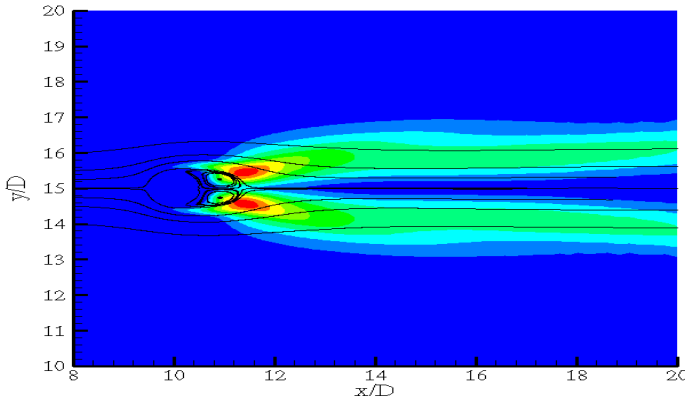
Fig. 5. Contours of root-mean square streamwise velocity fluctuation for the flow past a circular cylinder at Re=200. Contour levels used are: (0.1 to 0.45 in steps of 0.05). Also shown are the time-mean streamlines capturing the wake bubble.

Translating Rotating Circular Cylinder

In order to demonstrate the capability of the code to simulate flow with moving bodies, computations have been performed for a circular cylinder undergoing translating and rotational motion in a channel. The channel height is 4D with a length of 10D. At the inflow (x=0), a uniform free-stream velocity is imposed; at the bottom (y=0) and top (y/D=4), no-slip wall condition is applied; while a convective boundary condition is applied at the outflow (x/D=10) boundary. The initial cylinder center is located at (2D,2D). The circular cylinder has a nondimensional streamwise translational motion in the direction of the free-stream field of $(U_{trans}/U_\infty = 0.1)$ along with a nondimensional counterclockwise rotational motion of $(\omega R/U_\infty = 2.0)$. The Reynolds number ($\mathrm{Re} = U_\infty D/\nu$) considered has a value of 800. The computations are performed on a uniform 251x101 grid. Fig. 6 presents instantaneous contours of the spanwise vorticity (ω_z) at various time instances in the motion of the cylinder. The combined translation and rotation produces a complex topology of the shear layers on the cylinder surface. Note that in a typical body-conformal Lagrangian methodology, this simulation would have required the use of time-evolving complex mesh. This is quite easily avoided under the current approach and is completed in a very computationally efficient manner.
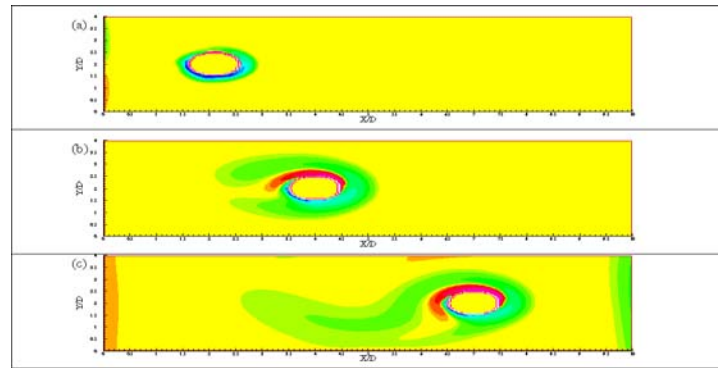
Fig. 6. Contours of instantaneous spanwise vorticity for a circular cylinder undergoing a streamwise translational and counterclockwise rotational motion in a channel at time instances (a) t=0.5, (b) t=10, and (c) t=25. Red (blue) values represent counterclockwise (clockwise) rotational motion. Initial cylinder center is located at (2D,2D).

Synthetic Jet

In addition to these canonical cases, numerical simulations of 3D synthetic jet have been performed. These devices have emerged as an important micro (or meso) fluidic device for thrust vectoring in jet engines, mixing enhancements and active control of separation and turbulence in boundary layers. The jet is created at the slot by an oscillating diaphragm attached to the bottom of the jet cavity. Fig. 7 shows two instantaneous flow visualizations of the flow for one case where a square jet slot is employed and they clearly indicate the formation of a strong jet and a coherent set of vortices. A comprehensive numerical investigation of this flow configuration is currently being carried out and these results will be reported elsewhere.

SUMMARY AND CONCLUSIONS

A computational technique has been developed to simulate the flow around complex bodies on fixed Cartesian grids. Embedded bodies are represented through "iblanking" of the cells inside the body; and therefore curved boundaries are represented in a stair-step fashion. Results obtained for the flow past a backward facing step and circular cylinder wakes indicate that the method is capable of providing a good prediction of complex geometry flows. Further, two relatively complex cases have been simulated to demonstrate the capabilities of the solver. The solver is currently being parallelized using OpenMP and MPI directives greatly facilitated by the use of the purely Cartesian grid, allowing more refined grids to be used for complex geometrical configurations

ACKNOWLEDGMENTS

REFERENCES

[1] Ye, T., Mittal, R., Udaykumar, H.S., and Shyy, W., 1999, "An Accurate Cartesian Grid Method for Viscous Incompressible Flows with Complex Immersed Boundaries," *J. Comp.Physics,* **156**, pp. 209-240.

[2] Chorin, A.J., 1967, "A Numerical Method for Solving Incompressible Viscous Flow Problems," *J. Comp. Phys.,* **2**, pp. 12-26.

[3] Mittal, R., and Balachandar, S., 1996, "Direct Numerical Simulation or Flow past Elliptic Cylinders," *J. Comp. Phys*., **124**, pp. 351-367.

[4] Mittal, R., 1999, "A Fourier-Chebyshev Spectral Collocation Method for Simulating Flow past Spheres and Spheroids," *Int. J. Num. Meth. Fluids*, **30**, pp. 921-937.

[5] Zang, Y., Streett, R.L., and Koseff, J.R., 1994, "A Non-Staggered Fractional Step Method for Time-Dependent Incompressible Navier-Stokes Equations in Curvilinear Coordinates," *J. Comp. Phys*., **114**, pp. 18.

[6] Balay, S., Gropp, W.P., McInnes, L.C., and Smith, B.F., 2000, "PETSc 2.0 Users Manual," Argonne National Laboratory, ANL-95/11-Revision 2.0.29

[7] Raju, R., 2002, Private communication, University of Illinois at Urbana-Champaign.

[8] Udaykumar, H.S., Mittal, R., Rampunggoon, P., and Khanna, A., 2001, "A Sharp Interface Cartesian Grid Method for Simulating Flows with Complex Moving Boundaries," J. Comp. Phys., **174**, pp. 345-380.

[9] Udaykumar, H.S., Mittal, R., and Rampunggoon, P., 2002, "Interface Tracking Finite Volume Method for Complex Solid-Fluid Interactions on Fixed Meshes," *Communications in Numerical Methods in Engineering*, **18**, pp. 89-97.

[10] Armaly, B.F., Durst, F., Periera, J.C.F., and Schonung, B., 1983, "Experimental and Theoretical Investigation of Backward-Facing Step Flow," *J. Fluid Mech*., **127**, pp. 473-496.

[11] Williamson, C.H.K., 1996, "Vortex Dynamics in the Cylinder Wake," *Ann. Rev. Fluid Mech*., **28**, pp. 477.

[12] Braza, M., Chassiang, P., and Ha Minh, H., 1986, "Numerical Study and Physical Analysis of the Pressure and Velocity Fields in the Near Wake of a Circular Cylinder," *J. Fluid Mech*., **165**, pp. 79.
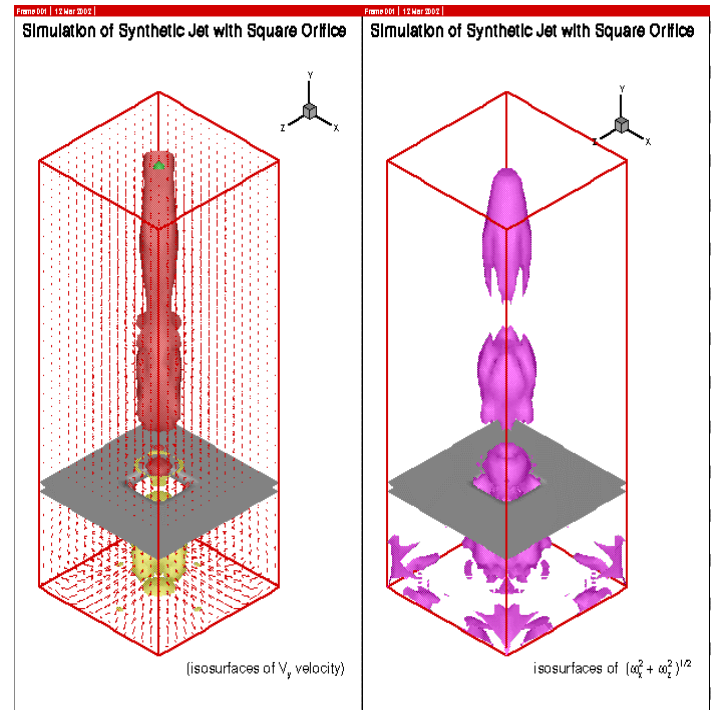
Fig. 7. Visualization of synthetic jet exiting a square orifice.